An efficient Non-Linear Chirp Scaling method of focusing bistatic SAR images

Yew Lam Neo
University of British Columbia, Canada

Frank Wong
MacDonald, Dettwiler and Associates Ltd., Canada

Ian Cumming
University of British Columbia, Canada

Abstract

Bistatic SAR data processing parameters, unlike monostatic SAR data, are generally azimuth-variant. The Non-Linear Chirp Scaling (NLCS) algorithm introduced in this paper is able to handle the azimuth variance. It focuses a bistatic image by first introducing a bulk linear range cell migration correction followed by a chirp scaling process to equalize the azimuth chirp rates for all targets in the same range gate. Efficiency is achieved by applying matched filtering in the azimuth frequency domain. A technique to perform image registration from the focused image to the ground plane is also discussed. This algorithm is verified with a simulation experiment.

1 Introduction

The NLCS algorithm has been shown to be an innovative way to focus bistatic SAR images. It is able to focus monostatic images and has been demonstrated to work on the bistatic configuration with a moving transmitter and a stationary receiver [1]. It is an efficient focusing algorithm that does not require any interpolation at the focusing stage. The algorithm has been extended to the case where both the receiver and the transmitter are moving in a parallel track with the same velocity [2], and imaging at a squinted angle.

Several bistatic processing methods have been proposed that may involve interpolation or numerical methods to solve the bistatic range equation and may even require the platforms to fly in more restrictive bistatic configurations. For instance, platforms are required to fly in parallel tracks with similar velocities [3], [4] and [5].

In this paper, the NLCS algorithm is discussed in Section 2. Registration to a flat earth model is introduced in Section 3. In Section 4, a simulation example is used to demonstrate the application of the algorithm.

2 NLCS Algorithm

The main steps of the NLCS algorithm are illustrated in **Figure 1**. The residual Quadratic Range Cell Migration (QRCMC) is an extended part of the original NLCS algorithm [1]. The first step of the algorithm is range compression. Linear Range Cell Migration (LRCM) exists which varies with range. However, this variation of LRCM is small; this is especially so for short wavelength systems. LRCM correction (LRCMC) using a linear interpolation step is applied after range compression, consequently targets with different FM rates fall into the same range gate. Then NLCS is applied to equalize their FM rates along each range gate by using a perturbation function. Once the azimuth FM rate is equalized for all range gates, azimuth compression can be carried out in the frequency domain to focus the image.

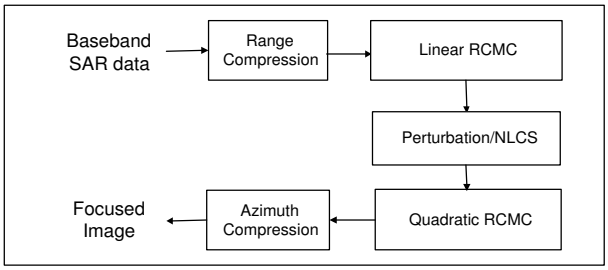

Figure 1: Extended NLCS Algorithm.

2.1 Signal model

For monostatic SAR, the trajectory of a point target is a hyperbola whereas that in bistatic SAR it is the sum of two hyperbolic ones. The instantaneous slant range to a point target for a bistatic configuration with reference to

Figure 2 is given by the range equation

$$R(\eta) = \sqrt{V_T^2\eta^2 + R_{Tcen}^2 - 2V_T\eta R_{Tcen}\sin(\theta_{sqT})} + \sqrt{V_R^2\eta^2 + R_{Rcen}^2 - 2V_R\eta R_{Rcen}\sin(\theta_{sqR})} \quad (1)$$

where η is the azimuth time, V_T is the velocity of the transmitter platform, and V_R is the velocity of the receiver platform. The other parameters are defined at the aperture center ($\eta = 0$): R_{Tcen} is the range of the transmitter to the point target and R_{Rcen} is the range of the receiver to the point target, θ_{sqT} is the squint angle of the transmitter, and θ_{sqR} is the squint angle of the receiver.

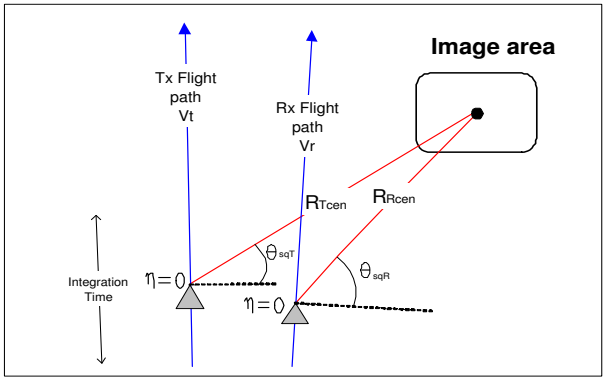

Figure 2: General Squinted Mode Bistatic Geometry.

We define the zero azimuth time being the midpoint of the integration path for the transmitter and receiver as shown in **Figure 2**. After demodulation, the received signal can be written in terms of the range fast time τ and azimuth slow time η,

$$s(\tau,\eta) = \rho_r(\tau - \frac{R(\eta)}{c})\, W_{az}(\eta)\exp(-j\,2\pi\frac{R(\eta)}{\lambda}) \quad (2)$$

where c is the speed of light and λ is the wavelength. The range envelope ρ_r is inversely proportional to the bandwidth of the transmitted pulse, and azimuth envelope W_{az} is determined by the composite antenna pattern in azimuth.

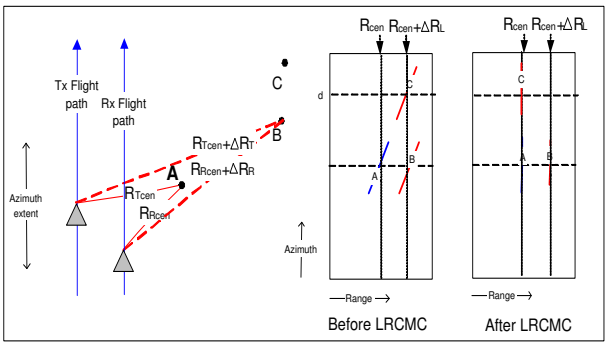

Figure 3: General Squinted Mode Bistatic Geometry.

Consider **Figure 3** with three point targets A, B and C on a flat earth. Targets A and B have the same beam (composite) center crossing time. Targets B and C have the same slant range from the flight paths. The time delay of the beam crossing of Target C from that of Target B is η_d. For processing purposes, we choose Target A to be the center of the image ($\eta_d = 0$).

In order to simplify the phase equations, we shall limit the phase equation of the received data up to the quadratic term for illustration purposes. This restriction can be lifted by inclusion of higher order terms.

2.2 Range cell migration correction

The first step in NLCS is the LRCMC. This can be done either using linear interpolation in the range-azimuth time domain or done together with range compression using a phase ramp in range frequency domain. The LRCMC step allows the NLCS to handle high squint cases.

QRCMC is done in the range-Doppler domain. For algorithms such as the range-Doppler in which RCMC is performed in the range-Doppler domain, serious range-Doppler coupling occurs and Secondary Range Compression (SRC) [7], [8] can be used to mitigate this coupling.

The signal for reference Target A after RCMC (linear and quadratic), ignoring the range envelope, is given by

$$s_{Apert}(\eta) = W_{az}(\eta) \exp\left\{-j\frac{\pi}{\lambda}\left[\frac{V_T^2\cos^2(\theta_{sqT})}{R_{Tcen}} + \frac{V_R^2\cos^2(\theta_{sqR})}{R_{Rcen}}\right]\eta^2\right\} \quad (3)$$

Targets B and C have similar phase characteristics for the parallel flight cases. The phase signal for Target B or Target C is

$$s_{Cpert}(\eta) = W_{az}(\eta-\eta_d) \exp\left\{-j\frac{\pi}{\lambda}\left[\frac{V_T^2\cos^2(\theta_{sqT})}{R_{TcenB}} + \frac{V_R^2\cos^2(\theta_{sqR})}{R_{RcenB}}\right](\eta-\eta_d)^2\right\} \quad (4)$$

For the non-parallel case, we still assume that the phases are similar and processing is done using invariance regions.

2.3 FM rate equalization

As shown in [2], a cubic phase perturbation function will be able to equalize the target FM rates along the azimuth. The perturbation function is $\exp(j\pi\alpha\eta^3)$, with the coeffi-

cient α given by

$$\alpha = \frac{1}{3}\left[\frac{V_T^2\cos^2(\theta_{sqT})}{\lambda R_{Tcen}R_{cen}} + \frac{V_R^2\cos^2(\theta_{sqR})}{\lambda R_{Rcen}R_{cen}}\right] \left[V_T\sin(\theta_{sqT}) + V_R\sin(\theta_{sqR})\right] \quad (5)$$

where R_{cen} is the sum of R_{Tcen} and R_{Rcen}.

2.4 Azimuth frequency matched filter

Once the azimuth FM Rates are equalized, all targets in the same range gate can be focused using the same matched filter.
The frequency matched filter can be obtained by first performing an azimuth Fourier transform on (3), giving

$$S_{mfA}(\tau, f_\eta) = \int s_{Apert}(\tau,\eta)\exp(j\pi\alpha\eta^3) \exp(-j2\pi f_\eta\eta)d\eta \quad (6)$$

The phase of the Fourier integral can be evaluated using the principal of stationary phase. The azimuth frequency f_η and azimuth time η are related by

$$f_\eta = -\frac{1}{\lambda}\left\{\frac{V_T^2\cos^2(\theta_{sqT})}{R_{Tcen}} + \frac{V_R^2\cos^2(\theta_{sqR})}{R_{Rcen}}\right\}\eta + \frac{3}{2}\alpha\eta^2 \quad (7)$$

The matched filter can be found by a reversion of power series formula given in [6] to obtain an expression of η in terms of f_η.

$$\eta(f_\eta) = A_1 f_\eta + A_2 f_\eta^2 + A_3 f_\eta^3 + ... \quad (8)$$

where

$$a_1 = -\frac{1}{\lambda}\left[\frac{V_T^2\cos^2(\theta_{sqT})}{R_{Tcen}} + \frac{V_R^2\cos^2(\theta_{sqR})}{R_{Rcen}}\right]$$
$$a_2 = \frac{3}{2}\alpha$$
$$A_1 = \frac{1}{a_1}, A_2 = -\frac{a_2}{a_1}, A_3 = \frac{2a_2}{a_1^5} \quad (9)$$

The frequency matched filter is the conjugate of S_{mfA} and is given by

$$h(f_\eta) = \exp\{-j\phi[\eta(f_\eta)]\} \quad (10)$$

$$\phi[\eta(f_\eta)] = \pi\alpha\eta^3(f_\eta) - 2\pi f_\eta\eta(f_\eta) - \frac{\pi}{\lambda}\left[\frac{V_T^2\cos^2(\theta_{sqT})}{R_{Tcen}} + \frac{V_R^2\cos^2(\theta_{sqR})}{R_{Rcen}}\right]\eta^2(f_\eta) \quad (11)$$

After applying the matched filter in the range Doppler domain, an inverse Fourier transform will give the final focused image in the slant range time and azimuth time domain.

3 Registration

Image registration maps the focused image $I_1(\tau,\eta)$ to a flat earth plane $I_2(x,y)$. The process involves two steps. First, positions of known grid points in $I_2(x,y)$ are mapped into $I_1(\tau,\eta)$. These grid points are chosen to be parallel and perpendicular to one of the platform path. Then an affine transformation [9] is used to map the rest of the points.

It should be noted that in practice, a user would require an image product in certain spatial ground coordinates. Therefore the processed image must be resampled to a ground coordinates grid required by the user. Thus, the registration steps here do not significantly increase the computational requirement as resampling is an integral step in the imaging process.

4 Simulation

An airborne simulation was performed with the following parameters: transmitter squinted at 40° and both platforms moving in a non-parallel configuration with lateral separation of 3 km, $V_t = 200$ m/s and $V_r = 220$ m/s parallel to transmitter. It is a C-band system with wavelength $\lambda = 0.06$ m, beamwidth $\theta_{3dB} = 1.9^\circ$, PRF = 195 Hz. The ground range resolution is 1.9 m and the ground azimuth resolution is 2.5 m. The imaged area consists of 25 point targets which are 250 m apart from one another in either direction, forming a 1 km $\times$ 1 km square patch. The square patch has two of the edges parallel to the transmitter flight path. Rectangular weighting for both azimuth and range processing was used.

The flight geometry is illustrated in **Figure 4**.

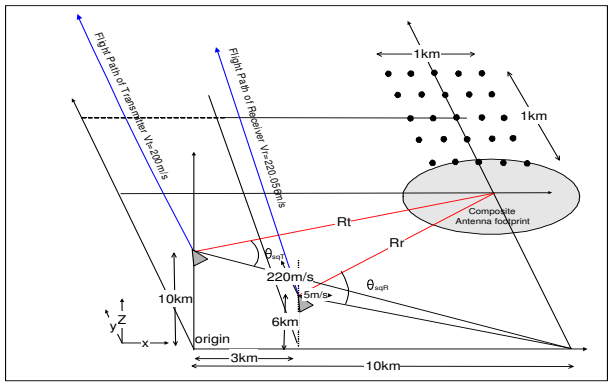

Figure 4: Flight geometry for simulation experiment

Figure 5 shows the image after performing focusing using the NLCS algorithm. Note that LRCMC introduced earlier in the NLCS process is reversed. The image is in slant range round trip time versus azimuth time.

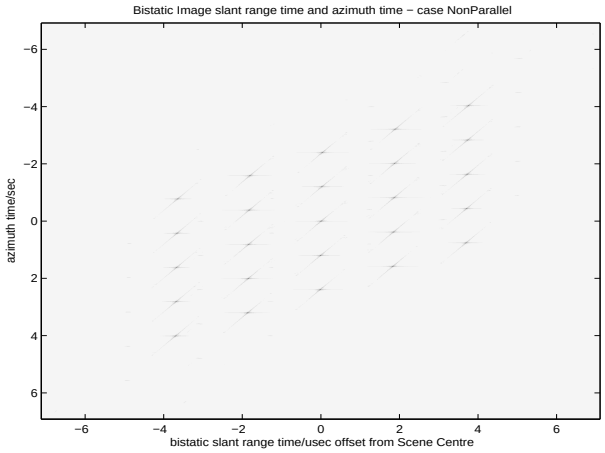

Figure 5: Focused image After performing NLCS

Figure 6 shows the results after affine transformation.

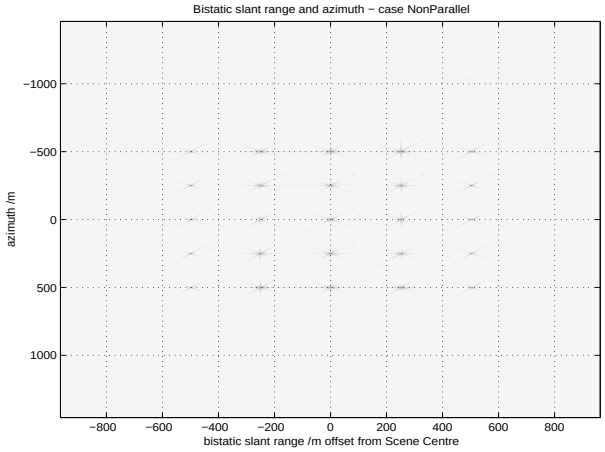

Figure 6: Final Registered image (linear line fit only)

The broadening is 5% or less for all the point targets. The theoretical range and azimuth Peak Side Lobe Ratio (PSLR) is -13 dB for a rectangular window. The measured PSLR for all targets is within 1 dB of this value. The measured range and azimuth registrations are within 0.5 and 0.1 m respectively.

5 Conclusion

The NLCS algorithm discussed in this paper is an extension on the original NLCS algorithm. The algorithm has several advantages. The algorithm is able to handle short wavelength systems where platforms are moving in a non-parallel configuration. Addition SRC is needed for long wavelength systems. The algorithm is able to handle high squint cases since it eliminates most of the range-Doppler coupling by using LRCMC. No interpolation is necessary in the focusing stage. It is able to focus bistatic data acquired on a non-parallel flight path. Efficiency is achieved by performing azimuth compression using a frequency matched filter. A simulation has been performed to verify the algorithm.

References

[1] F. H. Wong and T. S. Yeo. New Applications of Non-Linear Chirp Scaling in SAR Data Processing. *IEEE Trans. on Geoscience and Remote Sensing*, Vol. 39(5):946–953, May 2001.

[2] Y. L. Neo, I. G. Cumming, and F. H. Wong. Focusing Bistatic SAR Images Using Non-Linear Chirp Scaling. In *IEEE/URSI International Conference on Radar Systems RADAR'2004*, Toulouse, France, Oct 18-22, 2004.

[3] I. Walterscheid, J. H. G. Ender, A. R. Brenner, and O. Loffeld. Bistatic SAR processing using an $\omega - k$ type algorithm. In *Proc. Int. Geoscience and Remote Sensing Symp., IGARSS'05*, Seoul, Korea, August 2005.

[4] V. Giroux, H. Cantalloube, and F. Daout. An Omega-K algorithm for SAR bistatic systems. In *Proc. Int. Geoscience and Remote Sensing Symp., IGARSS'05*, Seoul, Korea, August 2005.

[5] D. D'Aria, A. Monti Guarnieri, and F. Rocca. Focusing Bistatic Synthetic Aperture Radar Using Dip Move Out. *IEEE Trans. on Geoscience and Remote Sensing*, Vol. 42(7):1362–1376, July 2004.

[6] H. B. Dwight. *Table of Integrals and Other Mathematical Data*. Macmillanc, New York, New York, 4th edition, 1961.

[7] M. J. Jin and C. Wu. A SAR Correlation Algorithm Which Accommodates Large Range Migration. *IEEE Trans. Geoscience and Remote Sensing*, Vol. 22(6):592–597, November 1984.

[8] I. G. Cumming and F. H. Wong. *Digital Processing of Synthetic Aperture Radar Data: Algorithms And Implementation*. Artech House, Norwood, MA, 2005.

[9] H. T. Croft, K. J. Falconer and R. K. Guy. *Unsolved Problems in Geometry*. Springer-Verlag, New York, NY, 1991.